Photovoltaic Properties of Doped Zinc Sulfide/n-Si Heterojunction Thin Films

Mahdi H. Suhail[1], Omed Gh. Abdullah[2,3,], Raoof A. Ahmed[4], Shujahadeen B. Aziz[2]*

[1] Department of Physics, College of Science, University of Baghdad, Baghdad, Iraq.
[2] Department of Physics, College of Science, University of Sulaimani, Sulaymaniyah, Iraq.
[3] Komar Research Center, Komar University of Science and Technology, Sulaymaniyah, Iraq
[4] Directorate of Education Salahuddin, Education Department of Tuz, Salahuddin, Iraq.
[*]E-mail: omed.abdullah@univsul.edu.iq

In this work, the current-voltage (I-V) characteristic curve of heterojunction solar cells based on pure ZnS and doped ZnS solid films have been studied. The films of pure and doped ZnS samples were deposited onto silicon substrates using the low-cost spray pyrolysis technique. Different weight ratios of Pb, Mn and Cu species were used for doping the ZnS films. The four-point probe electrical resistance technique has been used to measure thin films resistance, to evaluate the electrochemical performance of the hybrid solar cells. The photovoltaic properties and the forward I-V characteristics of the doped films were studied at room temperature. The solar cell efficiency, ideality factor, and other parameters were estimated. The results revealed that the efficiency, as well as the ideality factor, depends on the dopant concentration in the hybrid cells. The maximum power efficiency achieved was 3.5% at x=4% for $Zn_{1-x}S:Pb_x$, 1.84% at x=10% for $Zn_{x-1}S:Mn_x$, and 3.06% at x=8% for $Zn_{x-1}S:Cu_x$ structure.

1. INTRODUCTION

Among the various wide band-gap semiconductor materials zinc sulfide (ZnS) is an important II-VI group compound semiconductor, with a direct band-gap of 3.72 eV at ambient temperature, is regarded as one of the most promising materials for optoelectronic applications [1]. It is particularly suitable for use as a host material for a large variety of dopants because of its wide band gap [2]. As a wide band gap semiconductor, ZnS is a promising candidate for replacement of toxic cadmium sulfide

(CdS) in the buffer layer for $Cu(In,Ga)Se_2$ (CIGS) thin film solar cell application [3]. ZnS is an important material for diverse optoelectronic device applications such as sensors, electro-optic modulators, light-emitting diodes, n-type window layers in photovoltaic cells, and electroluminescent devices [2, 4-6].

Photovoltaics (PV) investigation attracted the attention of many researchers which is a direct means for detection and conversion of solar light into electrical energy at the atomic level [7, 8]. Alternative window materials layers have also been used as an effort to decrease the absorption loss in the window layer [9]. Various materials like ZnS, $Zn_xCd_{1-x}O$, $Cd_{1-x}Zn_xS$, and $ZnO_{1-x}S_x$ are among the alternative window layers that have been used instead of CdS [10]. A literature review reveals that the p-type semiconductors Cu_2ZnSnS_4 (CZTS) and $Cu_2ZnSnSe_4$ (CZTSe) have received much attention from researchers, and been considered as one of the most promising photovoltaic materials due to their small direct band gap [11, 12]. The CZTS and CZTSe thin-film solar cells with an absorber layer possess a bandgap in the range ~1 to ~1.5 eV [13, 14]. The highest values of power conversion efficiencies (PCEs) reported for pure CZTS, pure CZTSe and their mixture based solar cells have reached 8.4, 12.6 and 11.6%, respectively [15, 16]. Whereas, the maximum efficiency recorded for copper indium sulfide ($CuInS_2$) thin-film based solar cell is 12.5% for cells with the structure $Mo/CuInS_2/CdS/ZnO$, and in the case of using ZnS the best efficiency of about 7.8%, was recorded for the cell structure $Mo/CuInS_2/ZnS/ZnO$ [17]. Many researchers have reported that ZnS is one of the most efficient luminescent (phosphor) materials for solar cell applications in both the undoped and doped forms.

The extensive survey of the literature reveals that there are many methods for fabricating ZnS thin films such as spray pyrolysis, pulsed-laser deposition, spin coating, sputtering, sol-gel process, molecular beam epitaxy, and chemical bath deposition [18-21]. Among these techniques, spray pyrolysis is the best one suited for the preparation of ZnS thin films because of its simplicity and inexpensive experimental arrangement, vacuum less, high growth rate, ease of adding various doping materials, and the capability for homogeneous large-area coatings, which are desirable for the photovoltaic industries [22, 23]. Zhang et al. [24] theoretically investigate the influence of incorporation different divalent transition metals on the electronic structures of ZnS thin films. They found that the addition of dopant in ZnS films caused the increase of light absorption in the visible region, indicating the ability of preparation of a new solar cell prototypes [25]. In this study, to understand the importance of solid state parameter we deposited ZnS:Pb, ZnS:Mn and ZnS:Cu thin films onto glass substrates by an inexpensive, simple and easy deposition method, using spray pyrolysis technique. The main objective of this work is to investigate the dopant dependent current-voltage (I–V) characteristics of ZnS thin films experimentally.

2. EXPERIMENTAL

Solid films of pure ZnS and doped ZnS [$Pb_x ZnS_{(1-x)}$, $Mn_x ZnS_{(1-x)}$ and $Cu_x ZnS_{(1-x)}$ ($0.2 \leq x \leq 1$)] were grown onto silicon substrates by spray pyrolysis method at a fixed substrate temperature of 275 °C. The spraying solution was prepared by mixing the suitable quantity of dissolved zinc acetate

$Zn(CH_3COO)_2.2H_2O$ with thiourea $CS(NH_2)_2$. To prepare doped ZnS films different amounts of $Pb(CH_3COO)_2$, $MnCl_2.4H_2O$ and $CuCl_2.2H_2O$ were dissolved in distilled water separately as starting materials. The molar concentration of the solution was 0.1 Mole/Liter. The total solution (100 cm^3) was sprayed and controlled by a flow meter.

The compressed purified ambient air was used as the carrier gas with a pressure of 105 Pa. The solution sprays on a glass substrate for 2 seconds, and then the glass substrate left for 5 seconds until they return to their original temperature. This procedure was repeated several times for a preferred thickness. The substrates were heated using a simple electrical heating source, and the substrate temperature was controlled at 275 ^{o}C using an iron-constantan thermocouple. The thicknesses of the prepared thin-films were measured by Filmetrics (F20) equipment. The dark current at room temperature as a function of reverse-bias and forward-bias voltage in the range 3.0 to -3.0 V was measured for pure ZnS and doped ZnS structures using Keithley (typed 2425) programmable connected with Philips computer. From the plot of the forward current (I_f) versus applied forward-bias voltage (V_f), the values of ideality factor (β) have been calculated using the following equation [24]:

$$\beta = \frac{q}{k_B T} \frac{dV_f}{d\left[\ln\left(I_f / I_s\right)\right]} \qquad (1)$$

where q is carrier charge, k_B Boltzmann constant, T absolute temperature, and I_s is the saturation current which can be obtained by extrapolating the forward current curves to zero voltage. All of these should be defined for particular illumination condition. The illuminated I-V characteristics at room temperature were performed with intensities measured by solar meter using Kaiser Halogen lamp.

## 3. RESULTS AND DISCUSSION

3.1 Current-Voltage characteristics

The fabricated samples are tested for application as solar cell based materials. For this purpose, the deposited ZnS, $Pb_xZn_{1-x}S$, $Mn_xZn_{1-x}S$ and $Cu_xZn_{1-x}S$ ($0.2 \leq x \leq 1$) thin films were studied for current-voltage (I-V) characteristic curves for the range of ± 2 V, in the dark and under illumination. Figures (1, 2 and 3) show the variation of ($\ln(I)$) versus voltage (V) for pure ZnS, $Pb_xZn_{1-x}S$, $Mn_xZn_{1-x}S$ and $Cu_xZn_{1-x}S$ /n-Si heterojunction forward-bias voltage for different dopant content within the voltage range (0-2) Volt. It is obvious that the maximum I-V characteristic curve for Pb doping was achieved at 8 wt.%, while the maximum I-V curve for Mn doping is obtained at 2 wt.%, on the other hand, the for Cu doping the maximum was recorded at 4 wt.%.
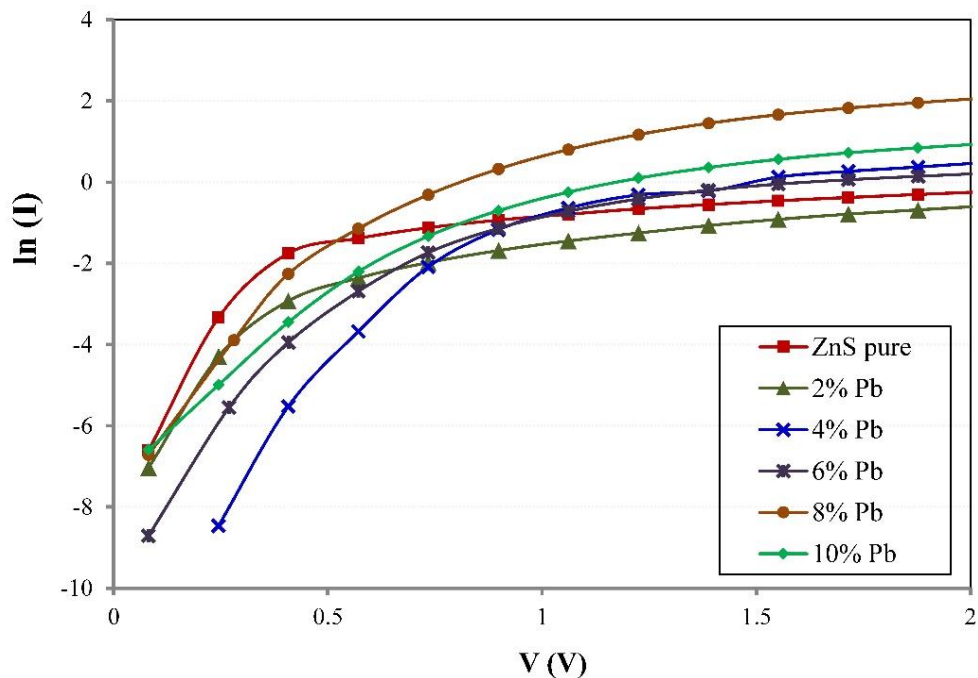
Figure 1. $\ln(I)$ versus V of the forward bias for pure ZnS and $Pb_x Zn_{1-x}S$/n-Si Heterojunction for different Pb content.
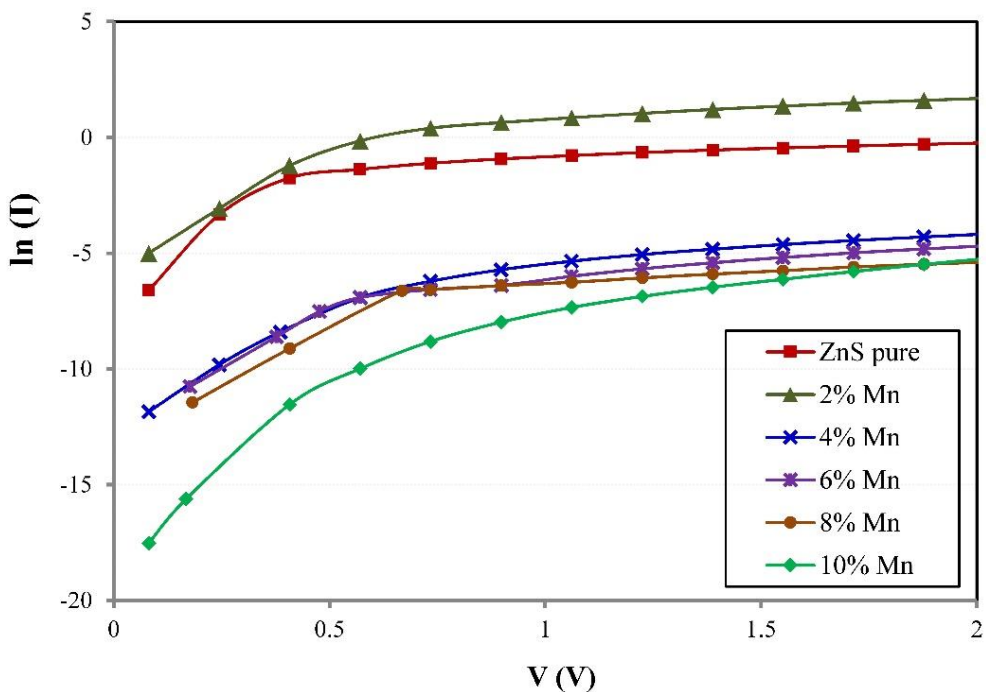
Figure 2. $\ln(I)$ versus V of the forward bias for pure ZnS and $Mn_x Zn_{1-x}S$/n-Si Heterojunction for different Mn content.
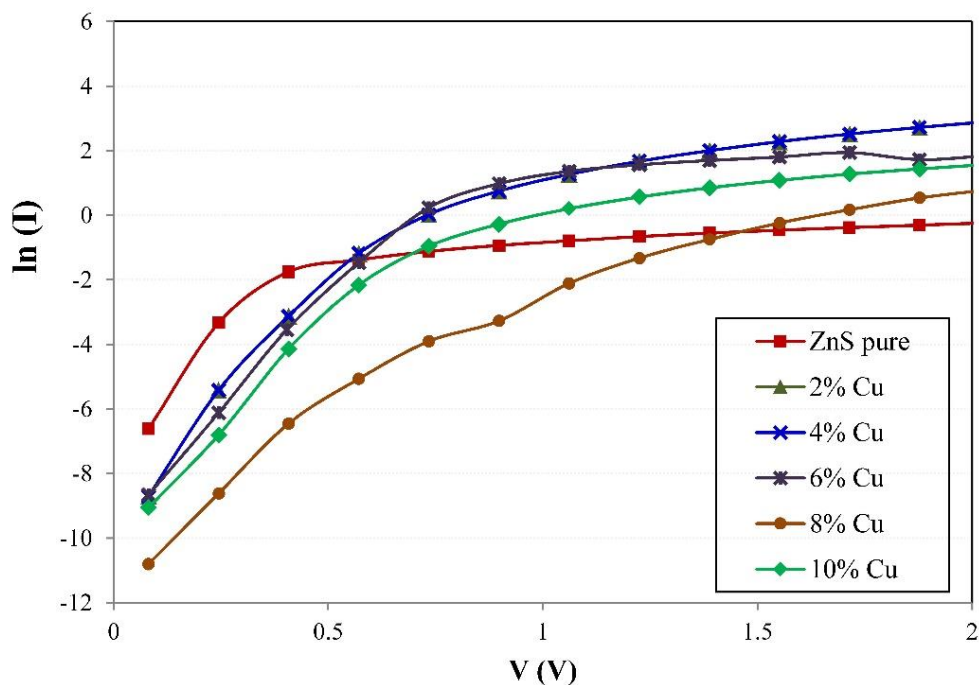
Figure 3. $\ln(I)$ versus V of the forward bias for pure ZnS and Cu_x $Zn_{1-x}S$/n-Si Heterojunction for different Cu content.

The current-voltage (I-V) characteristics of solar cells are an essential technique for the characterization of solar cells. It gives a good idea about the junction characteristics and different cell's parameters. Various models have been proposed to explain the solar cell experimentally observed behavior [27]. In general, the forward dark current is generated due to the flow of majority carriers where the applied voltage injects majority carriers lead to a decrease of the built-in potential and the width of the depletion region. When the concentration of majority and minority carrier are much higher than the intrinsic carrier concentration (*i.e* $n_p > n_i^2$) causes the generation of recombination current at low voltages (0-0.4) V. This is because the excited electrons from the valence band (V.B.) to the conduction band (C.B.) will recombine with the holes in the V.B., caused a little increase in the recombination current at low voltage region. While the tunneling current occurs in the higher voltages $(>0.4 \, Volt)$, where the current increases exponentially as the voltage increase. This current is known as the diffusion current, which dominates the process [28].

The initial part of Figures (1, 2 and 3) could be approximated by an expression of the type $I \sim \exp(qV / \beta k_B T)$. Thus the ideality factor (β) could be calculated from the slope of the initial linear region of the forward bias $\ln(I)$-V curve. It might be noted here that the ideality factor gives an indication of defects in the junction. In general, the ideality factor increase with an increase in the dopant content due to increasing of the structural defects accompanying the addition of Pb, Mn and Cu to ZnS as shown in Table 1.

Table 1. The values of ideality factor (β) for $Pb_xZn_{1-x}S$, $Mn_xZn_{1-x}S$ and $Cu_xZn_{1-x}S$ /n-Si Heterojunction.
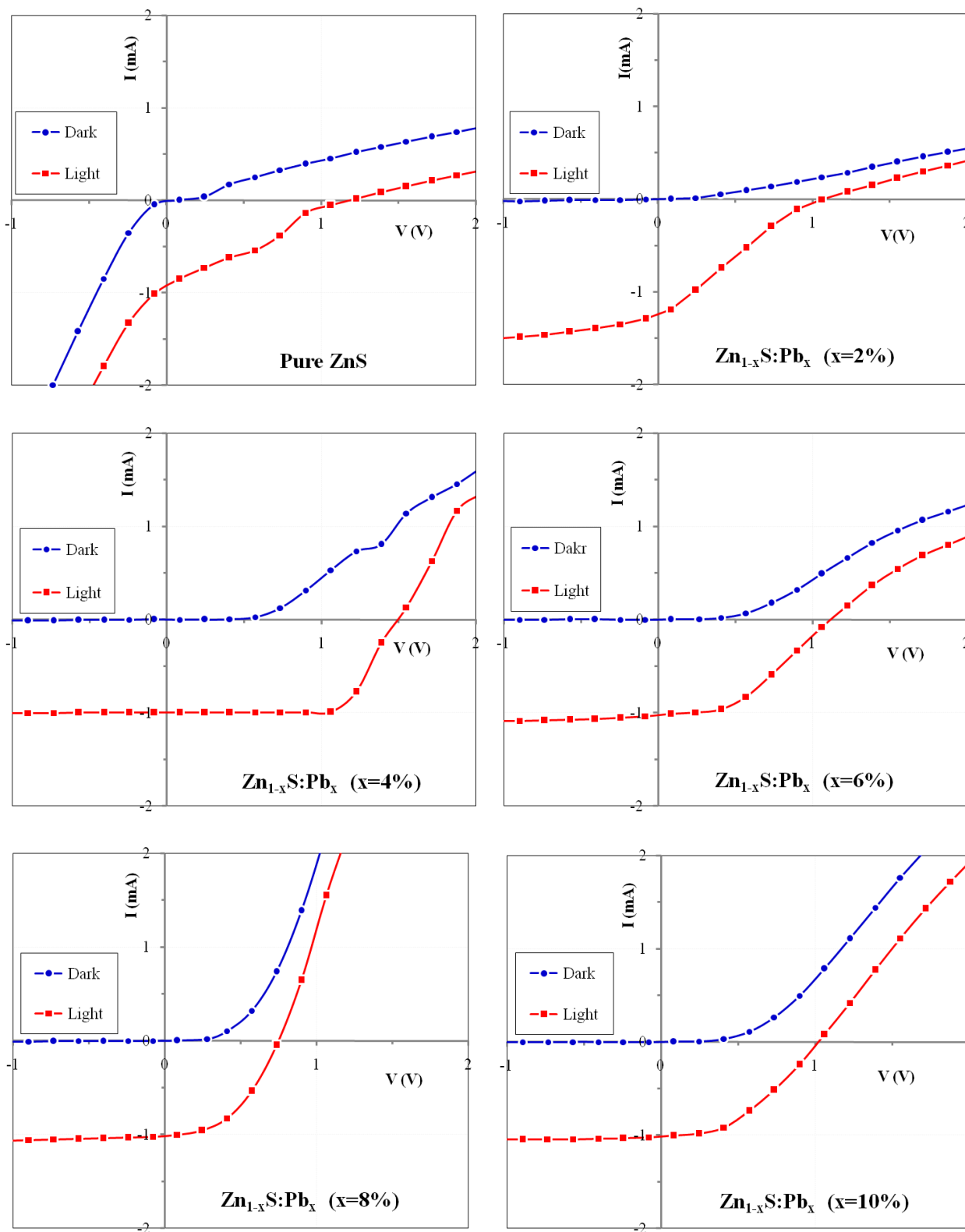
x%	$Pb_xZn_{1-x}S$		$Mn_xZn_{1-x}S$		$Cu_xZn_{1-x}S$	
	slope	B	slope	β	slope	B
0	14.89	2.69	14.89	2.69	14.89	2.69
2	17.13	2.33	11.58	3.45	12.60	3.18
4	17.12	2.34	11.35	3.52	10.52	3.80
6	15.89	2.52	10.79	3.71	14.71	2.72
8	13.34	3.00	9.93	4.03	13.72	2.92
10	15.10	2.70	18.07	2.21	9.63	4.15

The measured values of these parameters are slightly greater than their theoretical values which are a common fact found for many materials [29]. The I-V characteristics under illumination of the prepared thin films with different dopant content are presented in Figures (4, 5 and 6). The measurements were carried out in the dark and under illumination intensity equal to 30 mW/cm^2. Clearly, the photocurrent increases with an increase in the bias voltage. It is worth noting that the photocurrent in the reverse bias is larger than that in the forward bias. This is related to the fact that the width of the depletion region increases with increasing in reverse biased voltage, this leads to the formation of the electron-hole pairs across the interface. Thus the generation and diffusion of carriers increases. Consequently, the photocurrent which is a function of diffusion carriers is also increased [30].

3.2 Power output characteristics

The major crucial solar cell parameter is the maximum output power which is denoted by (P_m) as appeared in Eq. (2) [31]. The maximum output power is a crucial parameter because it has a significant effect on fill factor $(F.F)$. The $F.F$ of the solar cell is defined as the ratio of the maximum output power (P_m) to the product of the open circuit voltage (V_{oc}), and the short-circuit current (I_{sc}), as can be seen from the following equation:

$$F.F = \frac{P_m}{V_{oc} I_{sc}} \qquad (2)$$

Figure 4. I-V characteristic for pure ZnS and $Pb_xZn_{1-x}S/n$-Si heterojunction for different Pb content.
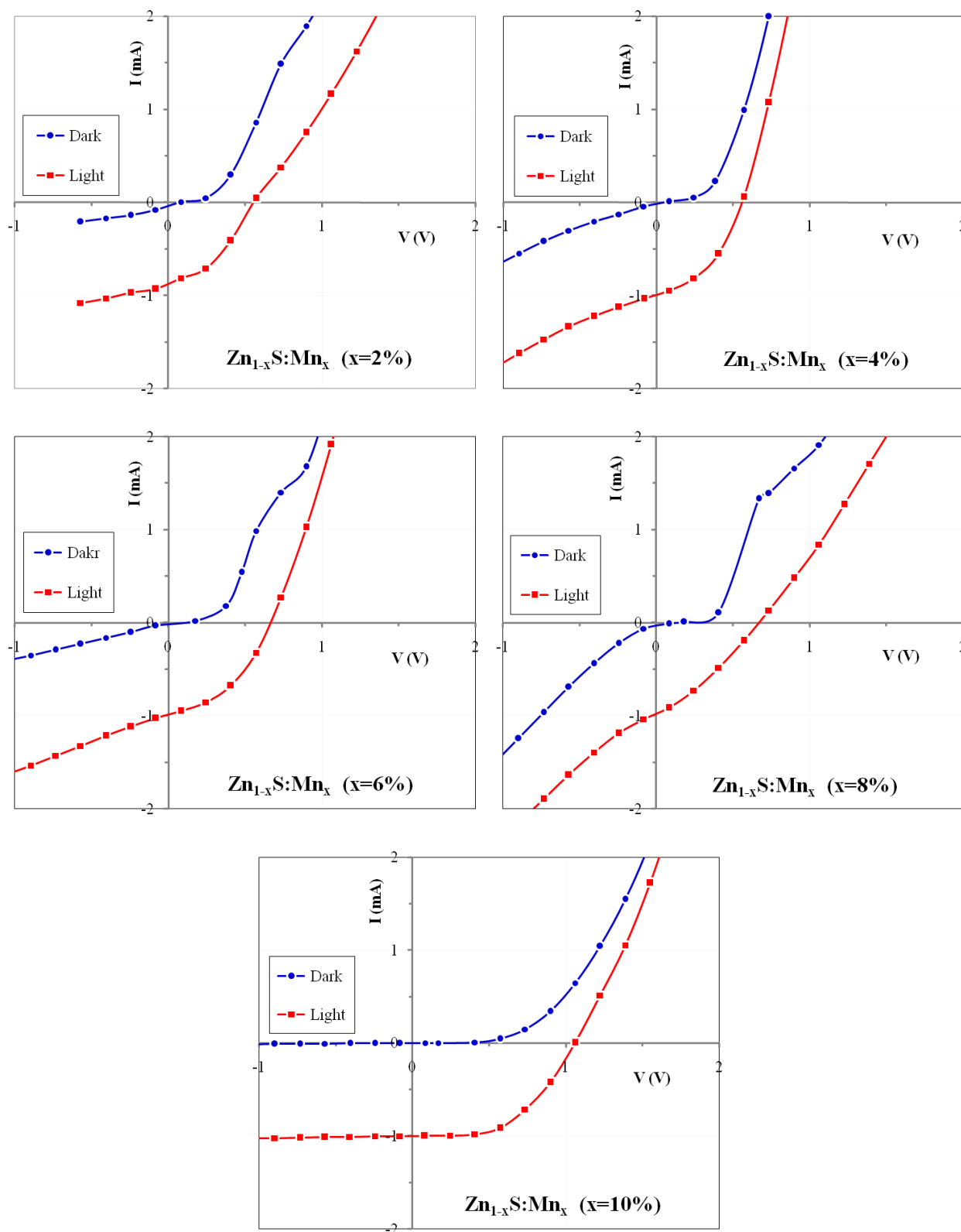
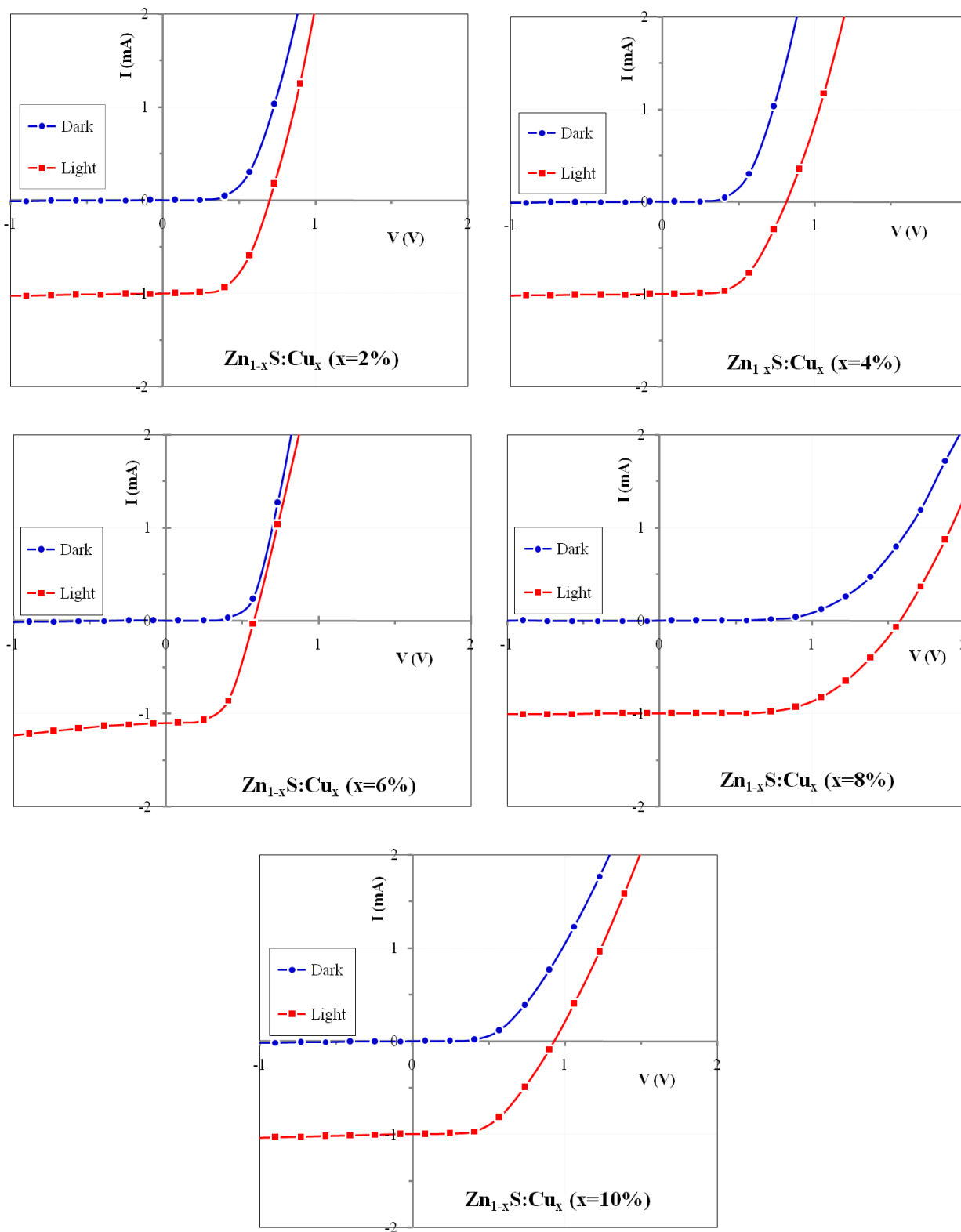**Figure 5.** I-V characteristic for $Mn_xZn_{1-x}S/n$-Si heterojunction for different Mn content.

Figure 6. I-V characteristic for $Cu_xZn_{1-x}S$/n-Si heterojunction for different Cu content.

The major weakness of these type of solar cells is the very low *F.F* values. The improvement in *F.F* values is a major challenge [32]. Another important parameter in determining the performance of photovoltaics is the power conversion efficiency (PCE). Photovoltaic (PV) devices with high conversion efficiency and low cost are expected for an extensive utilization of the solar energy in future [33]. The energy conversion efficiency ($\eta\%$) of the solar cell is defined as the ratio of the output power delivered to the operating point to the incident light power (P_{in}). Its value was estimated from this equation:

$$\eta = \frac{V_{oc}\ I_{sc}\ F.F}{P_{in}} \qquad (3)$$

These four quantities: I_{sc}, V_{oc}, *F.F*, and η are the critical performance characteristics of a solar cell [34].

Table 2. I-V parameters for $Pb_xZn_{1-x}S$, $Mn_xZn_{1-x}S$ and $Cu_xZn_{1-x}S$ /n-Si heterojunctions at difference dopant content.

x%	$Pb_xZn_{1-x}S$					
	I_{sc} (mA)	V_{oc} (V)	I_m (mA)	V_m(v)	F.F	$\eta\%$
0	0.94	1.20	0.52	0.60	0.28	1.04
2	1.24	1.05	0.65	0.50	0.25	1.08
4	1.00	1.50	1.00	1.05	0.70	3.50
6	1.02	1.10	0.90	0.52	0.42	1.56
8	1.00	0.75	0.70	0.50	0.47	1.17
10	1.20	1.02	0.90	0.40	0.29	1.20
x%	$Mn_xZn_{1-x}S$					
	I_{sc} (mA)	V_{oc} (V)	I_m (mA)	V_m(v)	F.F	$\eta\%$
0	0.94	1.20	0.52	0.60	0.28	1.04
2	0.90	0.55	0.58	0.35	0.41	0.68
4	1.00	0.55	0.70	0.38	0.48	0.89
6	1.00	0.65	0.55	0.50	0.42	0.92
8	1.00	0.65	0.55	0.40	0.34	0.73
10	1.00	1.05	0.85	0.65	0.53	1.84
x%	$Cu_xZn_{1-x}S$					
	I_{sc} (mA)	V_{oc} (V)	I_m (mA)	V_m(v)	F.F	$\eta\%$
0	0.940	1.200	0.520	0.600	0.277	1.040
2	1.00	0.70	0.85	0.48	0.58	1.36
4	1.00	0.80	0.88	0.50	0.55	1.47
6	1.10	0.58	0.90	0.40	0.56	1.20
8	1.00	1.58	0.85	1.08	0.58	3.06
10	1.00	1.00	0.82	0.59	0.48	1.61

All of these parameters should be defined for particular illumination conditions [35]. Table 2 summarizes the I-V characteristic parameters for all the fabricated solar cell devices. The power conversion efficiency (PCE) of the devices improved significantly from 1.04 % to 3.5% for ZnS film incorporated with 4 wt.% of Pb. This value is very close to that reported by Wen Ji et al. [36] for ZnS annealed at 250 $^{\circ}$C. The maximum efficiency of 1.8 % was achieved for ZnS doped with 10 wt.% of Mn salt. As well as the high efficiency of about 3.06% was recorded for ZnS containing 8 wt.% of Cu. The observed improvement in both photocurrent and photopotential response mainly attributed to the decreased series resistance, and increased photosensitivity.

4. CONCLUSION

The following conclusions were achieved for the fabricated solar cell devices. The doped ZnS films were deposited onto a silicon substrate using simple and inexpensive chemical spray method. The photovoltaic properties of the thin films have been analyzed. The photocurrent increases with increasing the positive bias voltage, and the photocurrent in the reverse bias is larger than that in the forward bias. This can be attributed to the fact that the depletion region width increases with increasing the reverse-bias voltage which causes the generation of the electron-hole pairs. The observed enhancements in the photopotential and photocurrent were attributed to the decreased series resistance and increased photosensitivity. The maximum efficiency for $Zn_{1-x}S:Pb_x$ was 3.5% at x=4%, for $Zn_{x-1}S:Mn_x$ was 1.84% at x=10%, and for $Zn_{x-1}S:Cu_x$ was 3.06% at x=8%.

References

1. L. Wang, M. Lu, X. Wang, Y. Yu, X. Zhao, P. Lv, H. Song, X. Zhang, L. Luo, C. Wu, Y. Zhang, and J. Jie, *J. Mater. Chem. A*, 2013 (2014) 1148.
2. S. Biswas, and S. Kar, *Nanotechnology*, 19 (2008) 045710 (11pp).
3. A. Wei, J. Liu, M. Zhuang, and Y. Zhao, *Mater. Sci. Semicon. Proc.*, 16 (2013) 1478.
4. S. Yamaga, A. Yoshokawa, and H. Kasain, *J. Cryst. Growth*, 86 (1988) 252.
5. T. Wada Y. Hashimoto, S. Nishiwaki, T. Satoh, S. Hayashi, T. Negami, and H. Miyake, *Sol. Energ. Mater. Sol. Cell.*, 67 (2001) 305.
6. A. Ennaoui, W. Eisele, M. Lux-Steiner, T.P. Niesen, and F. Karg, *Thin Solid Films*, 431-432 (2003) 335.
7. V.B. Pujari, D.J. Dhage, and L.P. Deshmukh, *Ind. J. Eng. Mater. Sci.*, 15 (2008) 275.
8. E.U. Masumdar, L.P. Deshmukh, S.H. Mane, V.S. Karande, V.B. Pujari, and P.N. Bhosale, *J. Mater. Sci. Mater. Electron.*, 14 (2003) 43.
9. S. Hossain, N. Amin, and T. Razykov, *Chalcogenide Lett.*, 8 (2011) 187.
10. O.K. Echendu, and I.M. Dharmadasa, *Energies*, 8 (2015) 4416.

11. S.N. Park, S.J. Sung, J.H. Sim, K.J. Yang, D.K. Hwang, J. Kim, G.Y. Kim, W. Jo, D.H. Kim, and J.K. Kang, *Nanoscale*, 7 (2015) 11182.
12. B.L. Guo, Y.H. Chen, X.J. Liu, W.C. Liu, and A.D. Li, *AIP Adv.*, 4 (2014) 097115.
13. M. Miyauchi, T. Hanayama, D. Atarashi, and E. Sakai, *J. Phys. Chem. C*, 116 (2012) 23945.
14. S. Bag, O. Gunawan, T. Gokmen, Y. Zhu, and D.B. Mitzi, *Chem. Mater.*, 24 (2012) 4588.
15. M.A. Akram, S. Javed, M. Islam, M. Mujahid, and A. Safdar, *Sol. Energ. Mater. Sol. Cells*, 146 (2016) 121.
16. M. Guo, X. Zhu, and H. Li, *J. Alloy. Compd.*, 657 (2016) 336.
17. C. Calderon, J.S. Oyola, P. Bartolo-Perez, and G. Gordillo, *Mater. Sci. Semicon. Proc.*, 16 (2013) 1382.
18. V.L. Gayou, B.S. Hernandez, M.E. Constantino, E.R. Andres, T. Diaz, R.D. Macuil, and M.R. Lopez, *Vacuum*, 84 (2010) 1191.
19. A. Goudarzi, G.M. Aval, R. Sahraei, and H. Ahmadpoor, *Thin Solid Films*, 516 (2008) 4953.
20. F. Ozutok, K. Erturk, and V. Bilgin, *Acta Phys. Pol. A*, 121 (2012) 221.
21. A. Derbali, A. Attaf, H. Saidi, H. Benamra, M. Nouadji, M.S. Aida, N. Attaf, and H. Ezzaouia, *Optik* 154 (2018) 286.
22. W. Daranfed, M.S. Aida, A. Hafdallah, and H. Lekiket, *Thin Solid Films*, 518 (2009) 1082.
23. E. Turan, M. Zor, A.S. Aybek, and M. Kul, *Thin Solid Films*, 515 (2007) 8752.
24. J. Zhang, J. Ding, J. Cao, and Y. Ahang, *J. Solid State Chem.*, 184 (2011) 477.
25. A. Axelevitch, and B. Apter, *Microelectron. Eng.*, 170 (2017) 39.
26. S.E. Iyayi, and A.A. Oberafo, *J. Appl. Sci. Environ. Mgt.*, 9 (2005) 143.
27. R.A. AbdelRassoul, *Renew. Energ.*, 23 (2001) 409.
28. M.A. Green, Solar Cells: Operating Principles, Technology and System Applications, Prentice-Hall, Inc., Englewood Cliffs, NJ, (1998).
29. M.A. Barote, A.A. Yadav, T.V. Chavan, and E.U. Masumdar, *Digest J. Nanometer. Biostruct.*, 6 (2011) 979.
30. G.F.A. Dibb, M.A. Muth, T. Kirchartz, S. Engmann, H. Hoppe, G. Gobsch, M. Thelakkat, N. Blouin, S. Tierney, M.C. Orozco, J.R. Durrant, and J. Nelson, *Sci. Rep.*, 3 (2013) 3335 (1-7).
31. T. Nakamura, M. Imaizumi, S. Sato, and T. Ohshima, *IEEE Phot. Spec. Conf.*, (2012) 13055710
32. O.K. Echendu, F. Fauzi, A.R. Weerasinghe, and I.M. Dharmadasa, *Thin Solid Films*, 556 (2014) 529.
33. D.L. Wang, H.J. Cui, G.J. Hou, Z.G. Zhu, Q.B. Yan, and G. Su, *Sci. Rep.*, 6 (2016) 18922 (1-10).
34. G. Nisato, D. Lupo, and S. Ganz, Organic and Printed Electronics: Fundamentals and Applications, Taylor & Francis Group, LLC (2016).
35. J. Nelson, The Physics of Solar Cells, Imperial College Press, UK (2007).
36. L.W. Ji, Y.J. Hsiao, I.T. Tang, T.H. Meen, C.H. Liu, J.K. Tsai, T.C. Wu, and Y.S. Wu, *Nanoscale Res. Lett.*, 8 (2013) 470 (1-6).